Open Access Journal

Journal of Power Technologies 94 (Nuclear Issue) (2014) 85–95

journal homepage:papers.itc.pw.edu.pl

Dry patch formation in diabatic annular two-phase flows

Henryk Anglart*

Institute of Heat Engineering, Warsaw University of Technology
21/25 Nowowiejska Street, 00–665 Warsaw, Poland

Abstract

Conditions for the formation of a stable dry patch in vertical annular two-phase flows in heated channels are investigated. An analytical model of the force balance for the leading edge of the liquid film is developed. In addition to surface tension, evaporation thrust and capillary forces, the model includes the effect of turbulence, the pressure gradient and the interfacial shear stress. Numerical evaluations are performed to validate the model and to indicate the importance of various factors on the dry patch stability and on the resulting minimum wetting rate of the liquid film. The analyses indicate that good agreement with measurements is obtained in the case of a stagnant patch formed on liquid film flowing down a vertical surface. It is shown that for low and moderate mass flow rate of the gas phase in vertical co-current annular flow, the force balance is dominated by the stagnation and the shear stress forces. With growing mass flow rate of the gas phase, the pressure gradient and the interfacial shear stress become increasingly important. As a result, in accordance with measurements, the predicted minimum flow rate of the liquid film at which the patch is re-wetted decreases.

Keywords: Dryout, Annular flow, Minimum Wetting Rate, Liquid Film

1. Introduction

The critical heat flux (CHF) is one of the major limiting factors when designing high performance heat exchangers, which are encountered in many industrial applications such as cooling systems of electronic devices, steam generators and fuel assemblies of nuclear reactors. In high quality two-phase flows, when the annular flow pattern prevails, the CHF occurs when the liquid film dries out and a permanent dry patch is formed. For that reason this type of CHF is often termed as dryout. Even though the dryout mechanism is quite well understood, there is still no consistent theory that is capable of predicting the occurrence of dryout in arbitrary geometry and under any flow conditions. As high precision predictions are required in the safety evaluations of nuclear reactors, we still rely on correlations derived from full scale experiments.

The key issue when predicting the occurrence of dryout in annular two-phase flows is to ascertain the conditions that are necessary for the creation of a permanent dry patch. The dry patch may appear, of course, as a result of complete evaporation of the liquid film. This hypothesis forms the basis of several existing phenomenological models, which use the mass balance equation for the liquid film to predict the location of the dry patch in places where the film completely disappears [1, 2]. There is, however, experimental evidence that dryout occurs even when the mass flow rate in the liquid film per unit perimeter is as high as 0.8 kg/m·s, [3]. This critical film

*Corresponding author
Email address: henryk@kth.se (Henryk Anglart*)

flow rate is virtually zero when flow quality is higher than 50%, but it rapidly increases when the quality decreases below that value. Thus, it seems plausible to argue that for dryout to occur it is necessary that: (a) the liquid film attains a minimum or "critical" flow rate at which the film breaks down, (b) a stable dry patch is created. The former may occur either spontaneously or due to the presence of disturbances in the liquid film. It should be noted that no dryout will occur if only condition (a) is satisfied. Fukano et al. [4] performed dryout experiments in channels with obstacles and reported that close to the CHF the heating surface was repeatedly dried out by evaporation of the liquid film and rewetted by the passage of disturbance waves. A stable dry patch was created and the onset of dryout was noted only after further increase of the heat flux.

The minimum stable film flow rate has been extensively investigated by several researchers. Hobler [5] proposed a theory where the minimum wetting rate of a film flowing down a vertical wall was derived from the minimum condition of the total energy of the liquid film. This approach was subsequently employed and extended by e.g. Bankoff [6], Mikielewicz and Moszynski [7], Doniec [8], El-Genk and Saber [9] and Mikielewicz et al. [10].

There are reasons to believe that the minimum stable film flow rate, as predicted by the total energy theory, is not applicable to CHF conditions in annular two-phase flows. Hewitt and Lacey [11] investigated the breakdown of the liquid film in annular air-water two phase flow. Their experiments indicate that films can exist in a meta-stable state and will not break down unless there is an external disturbance. Spontaneous breakdown of the film typically occurs at very low film mass flow rates. However, when a disturbance is present, film breakdown occurs at much higher film flow rates, resulting from the stability condition of the liquid film motion. Effects such as nucleation, Marangoni forces and evaporation on the interface may de-stabilize the liquid film and cause pre-mature breakdown.

The objective of the current analysis is to investigate the conditions under which a stable dry patch can exist in annular two-phase flow. Analyses by Hartley and Murgatroyd [12], and Zuber and Staub [13] are extended to include the effects of turbulence, the pressure gradient and the interfacial shear stress.

2. Velocity profile and forces acting on film

Various models have been developed to predict the stable condition of a dry patch. Hartley and Murgatroyd [12] proposed employing the force balance to predict a stagnation condition of the dry patch. The same approach was used later by Zuber and Staub [13] and McPherson [14], who added additional effects to the force balance such as resulting from the thermo-capillary, vapor thrust and drag forces.

The present approach enlarges on the ideas of the above cited work and includes the following new aspects:

- vertical climbing film on a heated wall,
- pressure drop in the channel and the interfacial shear stress,
- turbulent liquid film flow.

A stable dry patch in the liquid film will be formed when all forces acting on the leading edge of the liquid film are in balance. In the present model, the following forces are taken into consideration:

- the stagnation pressure force,
- the surface tension force,
- the thermo-capillary force,
- the vapor thrust force,
- the skin and the shape drag force.

Fig. 1 shows the assumed geometry of the leading edge of the liquid film flowing vertically up in a heated channel. A uniform film of an average thickness δ_c and velocity w approaches the leading edge between points A and C. The shape of the leading edge depends on the surface as well as on the hydrodynamic forces. At point A a stable vertex of the dry patch is formed. As the liquid film approaches this vertex, flow separates into rivulets which are formed on both sides of the dry patch.

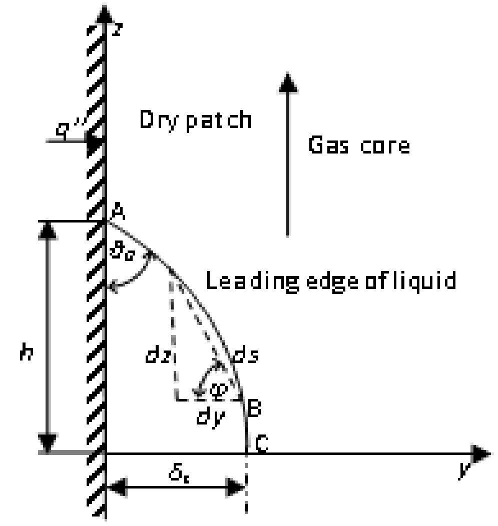

Figure 1: Leading edge of a liquid film upstream of a dry patch

The interface of the leading edge makes an angle θ_0 with the wall surface, which is equal to the contact angle at the prevailing local conditions. The height of the leading edge h is equal to the distance from point C, where the stable film exists to point A, where the stable dry patch vertex is formed. At any point B located at the interface between points A and C, the shape of the leading edge is characterized by the angle φ that a tangential to the interface makes with a line perpendicular to the wall surface. The forces acting on the leading edge of the liquid film will be expressed below in terms of the above mentioned parameters.

2.1. Velocity profile

For shear-driven laminar flow in the liquid film, the velocity distribution is obtained from solving the following differential equation, describing momentum conservation in the film,

$$-\frac{\partial p}{\partial z}+\mu_l\frac{d^2w}{dy^2}+\rho_l g_z=0 \tag{1}$$

with the following boundary conditions,

$$y=0 \;\Rightarrow w=0 \tag{2}$$

$$y=\delta \Rightarrow \mu_l\frac{dw}{dy}=\tau_i \tag{3}$$

The solution of Eqs. (1–3) is as follows,

$$w\left(y\right)=-\frac{\left(-\frac{\partial p}{\partial z}+\rho_l g_z\right)\delta^2}{2\mu_l}\left[\left(\frac{y}{\delta}\right)^2-2\frac{y}{\delta}\right]+\frac{\tau_i}{\mu_l}y \tag{4}$$

where p is the pressure, w is the local liquid film velocity, y is the distance from the wall, z is the distance along the wall, δ is the film thickness, ρ_l is the liquid density, μ_l is the liquid dynamic viscosity and g_z is the gravity acceleration along the wall surface.

For turbulent flow in the liquid film, the momentum equation and the boundary conditions are as follows,

$$-\frac{\partial p}{\partial z}+\frac{d}{dy}\left(\mu_{eff}\frac{dw}{dy}\right)+\rho_l g_z=0 \tag{5}$$

with the following boundary conditions,

$$y=0 \;\Rightarrow w=0 \tag{6}$$

$$y=\delta \Rightarrow \mu_{eff}\frac{dw}{dy}=\tau_i \tag{7}$$

here μ_{eff} is the effective dynamic viscosity, which is the sum of the molecular dynamic viscosity and the eddy viscosity. Various models can be applied to calculate this quantity. In general, the eddy viscosity in liquid films is evaluated using relations that were developed for turbulent flows in tubes. However, such models are not correct close to the liquid film interface, where turbulence damping is observed. In the present approach, the influence of the turbulence model is simulated by employing three different formulations: the mixing length model, the modified mixing length model with interface damping and the eddy viscosity model proposed by Blanghetti and Schlunder [15].

Employing the standard mixing length model, the effective viscosity is obtained as,

$$\mu_{eff}=\mu_l+\rho_l\kappa^2y^2\left|\frac{dw}{dy}\right| \tag{8}$$

where κ is the von Karman constant. In the modified mixing length approach, the damping at the interface is introduced as follows,

$$\mu_{eff}=\begin{cases}\mu_l+\rho_l\kappa^2y^2\left|\frac{dw}{dy}\right| & 0\le y\le\delta/2\\ \mu_l+\rho_l\kappa^2\left(y-\delta\right)^2\left|\frac{dw}{dy}\right| & \delta/2<y\le\delta\end{cases} \tag{9}$$

In the Blanghetti and Schlunder model, the effective viscosity is found as,

$$\mu_{eff}=\min\left(\mu_{eff1},\mu_{eff2}\right) \tag{10}$$

where

$$\mu_{eff1} = 0.5\mu_l \left\{ 1 + \left[1 + 0.64 y^{+2} \left(1 - e^{-y^{+2}/26} \right) \right]^{1/2} \right\} \tag{11}$$

$$\mu_{eff2} = \mu_l \left\{ 1 + \frac{0.0161\,\mathrm{Ka}^{1/3} Re_l^{1.34}}{\left(\nu_l^2/g\right)^{1/3}} \left[\frac{\tau(y)}{g(\rho_l-\rho_v)} + \delta \left(1 - \frac{y^+}{\delta^+} \right) \right] (\delta^+ - y^+) \right\} \tag{12}$$

Here the following dimensionless numbers are used,

$$\mathrm{Ka} = \frac{\rho_l^3 g^3 \left(\nu_l^2/g\right)^{1/3}}{\sigma} \tag{13}$$

$$Re_l = \frac{4\Gamma}{\mu_l} \tag{14}$$

where Γ is the film mass flow rate per unit wetted perimeter,

$$\Gamma = \rho_l \int_0^{\delta} w(y)\, dy \tag{15}$$

$\tau(y)$ is shear stress in liquid film,

$$\tau(y) = \tau_i - \left(\frac{\partial p}{\partial z} + \rho_l g \right) (\delta - y) \tag{16}$$

y^+ is the dimensionless distance from the wall,

$$y^+ = \frac{(\tau_w/\rho)^{1/2} y}{\nu_l} \tag{17}$$

δ^+ is the dimensionless film thickness,

$$\delta^+ = \frac{(\tau_w/\rho)^{1/2} \delta}{\nu_l} \tag{18}$$

ν_l is the kinematic viscosity of liquid, σ—surface tension, τ_w—wall shear stress, τ_i—interfacial shear stress, g—gravity acceleration.

The velocity distribution in the liquid film, $w(y)$, is obtained from a numerical integration of Eq. (5) with boundary conditions (6–7) and with the effective viscosity, μ_{eff}, determined by Eqs. (8–18). Both the stagnation force and the film flow rate are obtained numerically as well.

2.2. Stagnation force

The stagnation force per unit film perimeter acting in z-direction is given as follows,

$$F_{spz} = \frac{\rho_l}{2} \int_0^{\delta_c} w^2(y)\, dy \tag{19}$$

where $\delta = \delta_c$ is the critical film thickness at point C shown in Fig. 1. For shear-driven laminar flow, the force can be obtained in an analytical form as follows,

$$F_{spz} = \frac{\rho_l}{15} \left(\frac{-\frac{\partial p}{\partial z} + \rho_l g_z}{\mu_l} \right)^2 \delta_c^5 + \frac{5\rho_l \left(-\frac{\partial p}{\partial z} + \rho_l g_z \right) \tau_i}{24\mu_l^2} \delta_c^4 + \frac{\rho_l \tau_i^2}{6\mu_l^2} \delta_c^3 \tag{20}$$

In the case of turbulent flow a numerical integration is necessary, using the velocity profile obtained from a numerical solution of Eqs. (5–7), with the effective viscosity given by Eqs. (8–18).

2.3. Surface tension force

The surface tension force acting in z-direction is given as follows,

$$F_{stz} = \sigma_A \cos\theta_0 - \sigma_C \tag{21}$$

where θ_0 is the contact angle and σ_A, σ_C is the surface tension at points A and C, respectively, as shown in Fig. 1. Taking into account the temperature variation of the surface tension, the surface tension at point C can be expressed in terms of the surface tension at point A as follows,

$$\sigma_C = \sigma_A + \int_A^C \frac{\partial \sigma}{\partial s} ds = \sigma_A + \int_A^C \frac{\partial \sigma}{\partial T} \frac{\partial T}{\partial y} \frac{\partial y}{\partial s} ds = \sigma_A - \int_A^C \frac{\partial \sigma}{\partial T} \frac{q''}{\lambda_l} \cos\phi\, ds \tag{22}$$

where λ_l is the liquid thermal conductivity, T—liquid temperature, s—distance along interface, q''—heat flux, ϕ—interface inclination angle. Thus, combining Eqs. (21) and (22), the surface tension force becomes,

$$F_{stz} = \sigma_A (\cos\theta_0 - 1) + \int_A^C \frac{\partial \sigma}{\partial T} \frac{q''}{\lambda_l} \cos\phi\, ds \tag{23}$$

2.4. Thermo-capillary force

Due to heating the temperature of the interface may not be constant and the shear stress along the interface will be created as follows,

$$\tau_{tc} = \frac{\partial \sigma}{\partial s} \tag{24}$$

The differential thermo-capillary force acting on segment ds and projected onto z-direction is as follows,

$$dF_{tcz} = -dF_{tc} \sin\phi = -\frac{\partial \sigma}{\partial s} \sin\phi\, ds \tag{25}$$

Thus, the z-component of this force is obtained as,

$$F_{tcz} = -\int_A^C \frac{\partial \sigma}{\partial s} \sin\phi\, ds \tag{26}$$

2.5. Vapour thrust force

The net vapor thrust per unit perimeter and per a differential length of the interface ds is as follows,

$$dF_{vt} = \gamma'' (v_{vn} - v_{ln})\, ds \tag{27}$$

where γ'' is the evaporation rate per unit interface area and v_{vn}, v_{ln} are vapor and liquid velocities normal to the interface, respectively. Mass conservation on the interface yields, $\gamma'' = \rho_l v_{ln} = \rho_v v_{vn}$, and since, $v_{ln} = \rho v_{vn}/\rho_l$, the vapor thrust force projected onto z-direction becomes,

$$F = \int_A^C \gamma'' (v_{vn} - v_{ln}) \cos\phi ds = \int_A^C \rho_v v_{vn}^2 \left(1 - \frac{\rho_v}{\rho_l}\right) \cos\phi ds \tag{28}$$

The evaporation rate can be obtained from the energy balance as follows,

$$q'' dz = \gamma'' i_{fg} ds = \rho_v v_{vn} i_{fg} ds.$$

This equation can be written as,

$$v_{vn} = q'' dz/\rho_v i_{fg} ds = q'' \sin\phi/\rho_v i_{fg}.$$

Combining the above expression and substituting into Eq. (28) yields,

$$F_{vtz} = \int_A^C \rho_v \left(\frac{q''}{\rho_v i_{fg}}\right)^2 \left(1 - \frac{\rho_v}{\rho_l}\right) \sin^2\phi \cos\phi ds \tag{29}$$

2.6. Drag force

The total skin drag force acting in z-direction is obtained as,

$$F_{sdz} = -\int_A^C \tau_i \sin\phi ds \tag{30}$$

The total form drag force projected onto z-axis is as follows,

$$F_{fdz} = -\int_A^C p_{vi} \cos\phi ds \tag{31}$$

here p_{vi} is the vapor pressure at the interface.

The form drag force results from the pressure distribution along the leading edge of the liquid film. The vapor pressure distribution is approximated as,

$$p_{vi} = p_{vC} + \left(\frac{\partial p}{\partial z}\right)_C (z - z_C) \tag{32}$$

where $(\partial p/\partial z)_C$ is the total pressure gradient in z-direction in the channel at location C. In writing Eq. (32) it is assumed that the pressure in the gas core changes linearly with the pressure gradient evaluated at point C. Thus, the form drag force is as follows,

$$F_{fdz} = -\int_A^C \left[p_{vC} + \left(\frac{\partial p}{\partial z}\right)_C (z - z_C)\right] \cos\phi ds = -\int_A^C \left(\frac{\partial p}{\partial z}\right)_C (z - z_C) \cos\phi ds = -\left(\frac{\partial p}{\partial z}\right)_C \int_A^C (z - z_C) \cos\phi ds \tag{33}$$

3. The force balance

The formulation of the force balance requires information on the shape of the interface along the leading edge of the liquid film, which, in principle, is part of the solution. Strictly speaking this shape can be obtained from a solution of the Laplace relationship between the pressure difference over the interface and the interface curvature. However, it is expected that the results of such analysis would heavily depend on the assumed pressure distributions along the interface. Since these pressure distributions are not well determined, it is thus justified to employ an approximation in which the radius of the curvature of the interface results from the contact angle and the critical film thickness, as shown in Fig. 2.

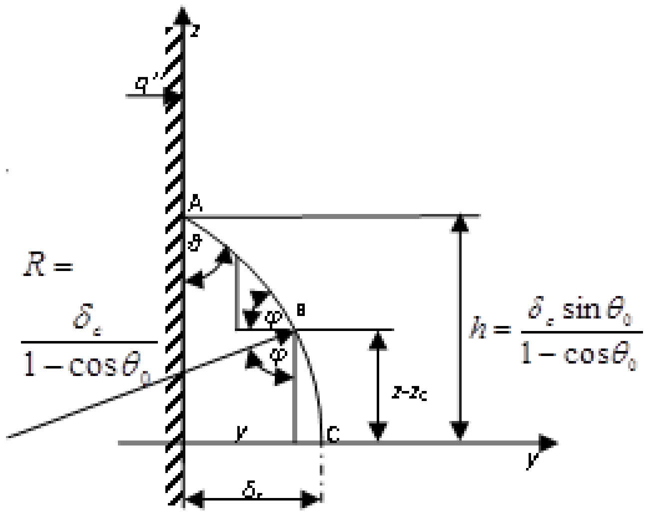

Figure 2: Assumed curvature of the leading edge of the liquid film

An additional advantage of the present approximation is that an analytical expression for the force balance can be obtained which is necessary to discern the importance of various effects.

With this assumption, the forces are as follows:

- the stagnation force is given by Eq. (20) and it does not depend on the shape of the leading edge of the liquid film,
- the surface tension force, Eq. (23), depends on the shape of the leading edge and becomes,

$$F_{stz} = \sigma_A (\cos\theta_0 - 1) + \frac{\partial\sigma}{\partial T}\frac{q''}{\lambda_l}\delta_c \qquad (23a)$$

- the thermo-capillary force, Eq. (26), is as follows

$$F_{tcz} = \frac{d\sigma}{dT}\frac{q''}{\lambda_l}\frac{\delta_c}{2}(1+\cos\theta_0) \qquad (26a)$$

- the vapor thrust force (Eq. 29) becomes,

$$F_{vtz} = \rho_v \left(\frac{q''}{\rho_v i_{fg}}\right)^2 \left(1 - \frac{\rho_v}{\rho_l}\right)\frac{\delta_c}{3} \times \left(1 + \cos\theta_0 + \cos^2\theta_0\right) \qquad (29a)$$

- the skin drag force, Eq. (30), is as follows,

$$F_{sdz} = \frac{\tau_i \delta_c \sin\theta_0}{1 - \cos\theta_0} \qquad (30a)$$

1. the form drag (Eq. 33) becomes,

$$F = -\left(\frac{\partial p}{\partial z}\right)_C \frac{1}{2(1-\cos\theta_0)^2} \times [\theta_0 - \cos\theta_0 \sin\theta_0]\,\delta_c^2 \qquad (33a)$$

The force balance for the leading edge of the liquid film is as follows,

$$F_{spz} + F_{stz} + F_{tcz} + F_{vtz} + F_{sdz} + F_{fdz} = 0 \qquad (34)$$

In the case of laminar flow, the force balance can be written explicitly in terms of the critical film thickness by substituting Eqs. (20), (23a), (26a), (29a), (30a) and (33a) into (34) as follows,

$$\frac{\rho_l}{15}\left(\frac{-\frac{\partial p}{\partial z}+\rho_l g_z}{\mu_l}\right)^2 \delta_c^5 + \frac{5\rho_l\left(-\frac{\partial p}{\partial z}+\rho_l g_z\right)\tau_i}{24\mu_l^2}\delta_c^4 + \frac{\rho_l \tau_i^2}{6\mu_l^2}\delta_c^3 - \left(\frac{\partial p}{\partial z}\right)_C \frac{1}{2(1-\cos\theta_0)^2}[\theta_0 - \cos\theta_0\sin\theta_0]\,\delta_c^2 + \left[\frac{\partial\sigma}{\partial T}\frac{q''}{\lambda_l}\frac{(1-\cos\theta_0)}{2} - \rho_v\left(\frac{q''}{\rho_v i_{fg}}\right)^2\left(\frac{\Delta\rho}{\rho_l}\right)\frac{\left(1+\cos\theta_0+\cos^2\theta_0\right)}{3} + \frac{\tau_i\sin\theta_0}{1-\cos\theta_0}\right]\delta_c + \sigma(\cos\theta_0 - 1) = 0 \qquad (34a)$$

For shear-driven turbulent flow in the liquid film, the force balance is obtained by substituting Eqs. (19), (23a), (26a), (29a), (30a) and (33a) into (34) as follows,

$$\frac{\rho_l}{2}\int_0^{\delta_c} w^2(y)\,dy - \left(\frac{\partial p}{\partial z}\right)_C \frac{1}{2(1-\cos\theta_0)^2}[\theta_0 - \cos\theta_0\sin\theta_0]\,\delta_c^2 + \left[\frac{\partial\sigma}{\partial T}\frac{q''}{\lambda_l}\frac{(1-\cos\theta_0)}{2} - \rho_v\left(\frac{q''}{\rho_v i_{fg}}\right)^2\left(\frac{\Delta\rho}{\rho_l}\right)\frac{\left(1+\cos\theta_0+\cos^2\theta_0\right)}{3} + \frac{\tau_i\sin\theta_0}{1-\cos\theta_0}\right]\delta_c + \sigma(\cos\theta_0 - 1) = 0 \qquad (34b)$$

Equation (34a) is a 5th degree polynomial that describes the dry patch stagnation condition in annular two-phase flow with heating. The real and positive root of the polynomial gives the minimum, or critical, film thickness at which the dry patch will remain stable. Correspondingly, Eq. (34b) can be solved iteratively to obtain the value of the minimum film thickness in the case of turbulent flow in the liquid film. In the following section predictions are compared with experimental data and the significance of various effects and their influence on minimum film thickness are presented.

4. Comparison with experimental data

The model given by Eq. (34a) was compared with available measured data and with selected analytical models. Experimental data with measured minimum film thickness for vertical boiling two-phase annular up-flow could not be found. Most of the data are obtained for adiabatic liquid films flowing down [16, 17]. Hewitt and Lacey [11] measured the minimum wetting rate for a climbing film, in which a dry patch was created by blowing air. It should be mentioned that the predictive accuracy of the minimum wetting rate strongly depends on the accuracy of the corresponding contact angle used in calculations. In most cases the equilibrium contact angle is measured, whereas very little is known about the dynamic contact angle, in particular at the leading edge of liquid film with evaporation. Ponter et al. [17] measured the minimum wetting rate for liquid films flowing down stainless steel, copper and Perspex surfaces. They also provide data for the equilibrium contact angle for various temperatures and surface conditions. Fig. 3 shows the predicted minimum wetting rate using Eq. (34a) compared with the measured data. Predictions obtained from models given by El-Genk and Saber [9] and Ponter et al. [16] are shown as well.

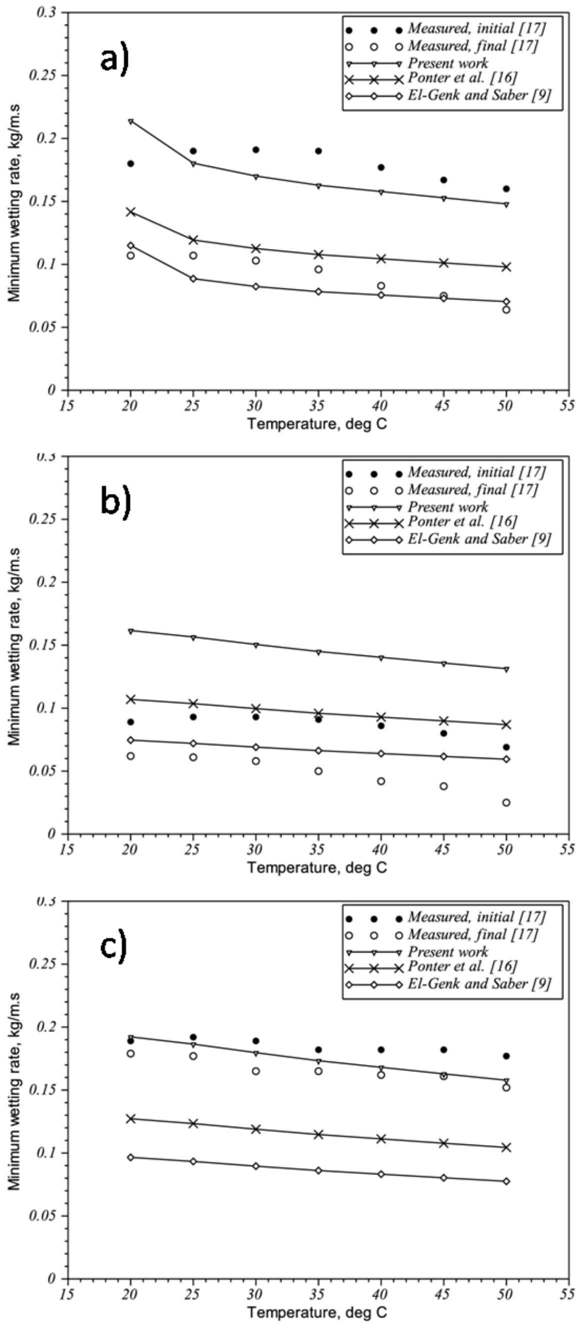

Figure 3: Prediction of the minimum wetting rate of liquid film flowing down a: copper surface (a), tainless steel surface (b), Perspex surface (c)

As shown in the figures, the present predictions are in good agreement with the measured data. For the copper and the Perspex surfaces the predicted minimum wetting rate of the liquid film stays between the measured initial and final wetting rates, while for the stainless steel surface the predicted minimum wetting rate is higher than both these values. It should be noted that in all calculations an equilibrium static contact angle was used. A certain discrepancy between measurements and predictions is observed for low temperatures, in the range from 20 to 30°C, where the measured minimum wetting rate stays constant or increases slightly with increasing temperature. All presented models predict a decreasing minimum wetting rate in the whole temperature range. This is due to the fact that the contact angle linearly decreases with increasing temperature at a rate of $-0.1°/°C$, [16]. The reason why the measured minimum wetting rate stays constant or increases with temperature in the range from 20 to 30°C is unknown.

Hewitt and Lacey [11] measured the minimum wetting rate of a climbing liquid film for adiabatic air-water annular two-phase flow in a vertical 12.7 mm/31.75 mm annulus. The dry patch was created artificially by blowing air on the wall covered with the liquid film. The flow rate of the liquid film was decreased until the dry patch could not be rewetted. Hewitt and Lacey [11] compared the measurements with their own calculations based on the model by Hartley and Murgatroyd [12] and concluded that the predictions in general gave much higher values of the minimum wetting rate than were observed in the measurements. The predictions could be matched with the measurements only if the contact angle was assumed to be equal to 17°C in the calculations. That was a much lower value than the static contact angle of 46°C measured by the same authors for relevant conditions. Hewitt and Lacey suggested that the discrepancy between the predictions and measurements could be due to the fact that the model lack an aerodynamic force acting on the leading edge of the liquid film. Another explanation could be that the Hartley and Murgatroyd's model assumes laminar flow in the liquid film, whereas the flow was turbulent in the experiments.

A comparison of the present model given by Eq. (34a) with Hewitt and Lacey data is shown in Fig. 4.

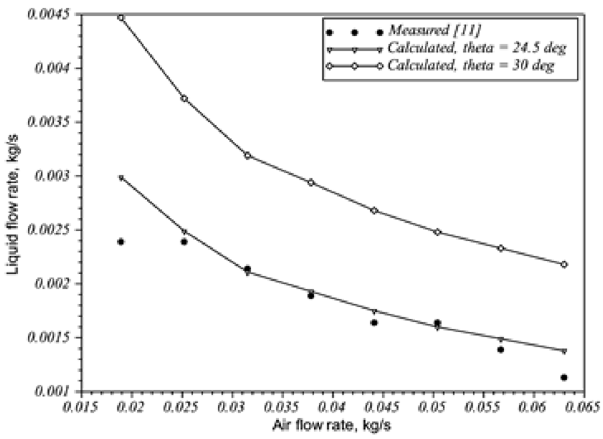

Figure 4: Minimum liquid film flow rate as a function of air flow rate. Comparison of predictions with experimental data [11]

As can be seen, the experimental data can be matched by the predictions when the contact angle is assumed equal to 24.5°C. Increasing the contact angle to 30°C gives the minimum wetting rate which is approximately 50% higher than the measured rate. In spite of this discrepancy, the model correctly predicts decreasing minimum liquid flow rate with increasing air flow rate. In that respect, the present results are consistent with the results reported by Hewitt and Lacey. However, due to the inclusion of the shape and skin drag forces acting on the leading edge of the liquid film, some improvement can be noticed.

Since the results shown in Fig. 4 were obtained by employing the laminar film flow model, a relevant question is whether such approximation is admissible for the present conditions. Various turbulence models were employed to investigate the effect of turbulence on the results of predictions. Fig.s 5(a-c) show the velocity profiles, minimum re-wetting liquid film Reynolds number and the relative stagnation force (ratio of the stagnation force to the surface tension force) obtained with the laminar and the three turbulence models described in Section 2.1.

Fig. 5(a) indicates that the velocity profiles for laminar flow as well as for turbulent flow using the viscosity model given by Blanghetti and Schlunder [15] are similar. The mixing length and the modified mixing length models predict more flat velocity distributions due to a higher value of the turbulent viscosity.

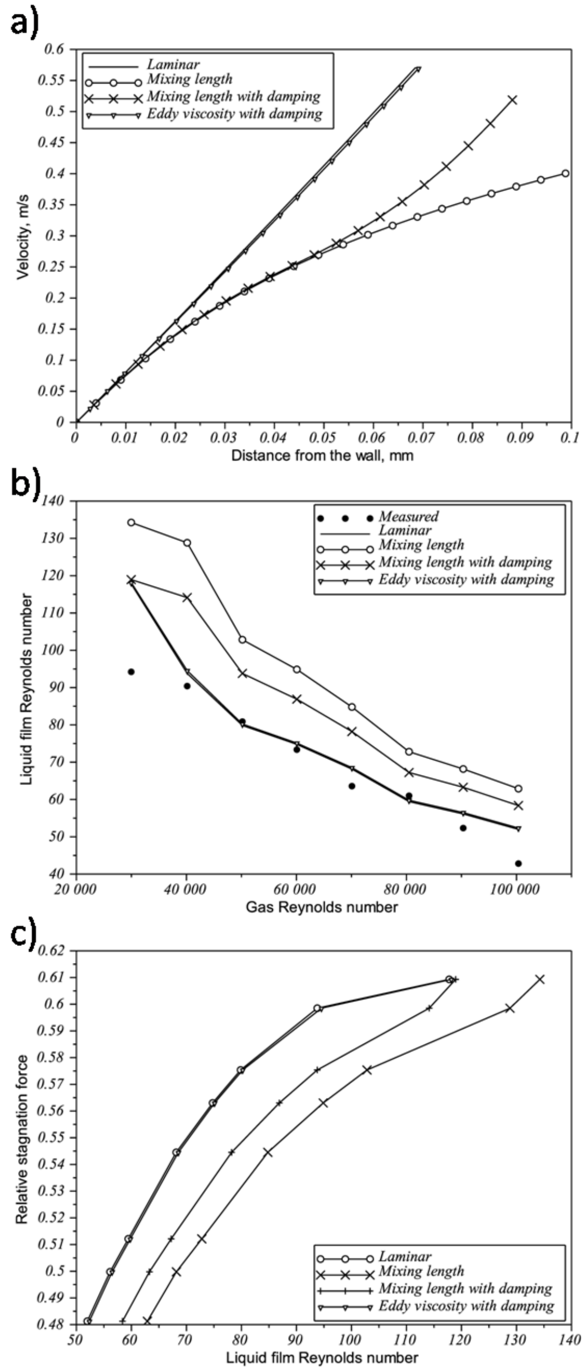

Figure 5: Influence of turbulence models on dry patch re-wetting in air-water annular flow in 12.7 mm/31.75 mm annulus at atmospheric pressure and contact angle 24.5°C: velocity profiles in liquid film (a), minimum re-wetting liquid film Reynolds number as a function of gas Reynolds number (b), ratio of stagnation force to surface tension force as a function of the liquid film Reynolds number (c)

As a result, the liquid film thickness increases, when the total mass flow rate is kept constant.

Fig. 5(b) shows that the minimum film Reynolds number, corresponding to the minimum wetting rate, predicted with the laminar flow assumption is very close to the results obtained with the Blanghetti and Schlunder [15] turbulence model. At the same time, the mixing length and the modified mixing length models yield higher values of the minimum film Reynolds number. This leads to a conclusion that the discrepancy between measurements and predictions for the Hewitt and Lacey data is not caused by the neglect of turbulence in the liquid film, since the increasing level of turbulence shifts the predicted minimum film Reynolds number (and thus the minimum re-wetting rate) further away from the measured values.

Fig. 5(c) shows the magnitude of the relative stagnation force, defined as the ratio of the stagnation force to the surface tension force, as a function of the liquid film Reynolds number. As expected, this force increases as the film Reynolds number increases. It can also be seen that this force decrease for turbulent films, while the film Reynolds number is kept constant. This is due to the increasing thickness and the decreasing flow velocity in liquid films with the increasing level of turbulence.

5. Significance of various effects

The stagnation force plays an important role in dry patch stability, as indicated in Fig. 5(c). The significance of this force was evaluated using as a reference the experimental data obtained by Hewitt and Lacey [11].

Fig. 6 shows that the significance of the stagnation force in the force balance decreases as the gas Reynolds number increasing. For low gas Reynolds numbers in a range of $\sim 3 \cdot 10^4$, the stagnation force corresponds to 61% of the surface tension force.
With an increasing Reynolds number, this ratio decreases and drops below 50% when the gas Reynolds number is larger than $\sim 9 \cdot 10^4$. This is due to the fact that with increasing gas flow rate, the importance of the skin and shape drag forces increases.

Fig.s 7 show the magnitude of various forces in relation to the surface tension force for contact angle in a range from 15 to 65°C. The calculations are per-

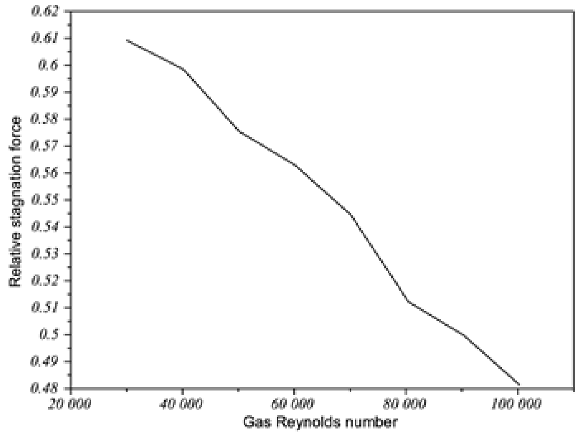

Figure 6: Ratio of stagnation force to surface tension force versus gas Reynolds number for air-water annular flow in 12.7 mm/31.75 mm annulus at atmospheric pressure; contact angle 24.5°C

formed for a water-steam mixture flowing at constant pressure gradient, interfacial shear stress and wall heat flux and at various system pressures from 2 to 12 MPa. In the whole range of pressure and contact angle the prevailing forces are due to stagnation pressure, skin drag and thermo-capillary effects, whereas the form drag and the vapor thrust forces are negligibly small. As can be seen, the magnitude of relative stagnation and thermo-capillary forces increase with increasing contact angle, whereas the magnitude of relative skin drag force decreases with increasing contact angle.
Fig.s 8 show the relative magnitude of various forces as a function of the wall heat flux and at different system pressures. As can be seen, the thermo-capillary force linearly increases with the heat flux. This effect is compensated with increasing magnitude of the relative stagnation force. As pressure increases from 2 to 12 MPa, the thermo-capillary force increases from 25 to 70% of the surface tension force, when the wall heat flux is equal to 2.5 MW/m^2.

6. Conclusions

An analysis is presented that predicts the conditions which allow for the formation of a stable dry patch in diabatic annular two phase flows. The analysis employs a force balance formulated for the leading edge of the liquid film. In addition to stagnation,

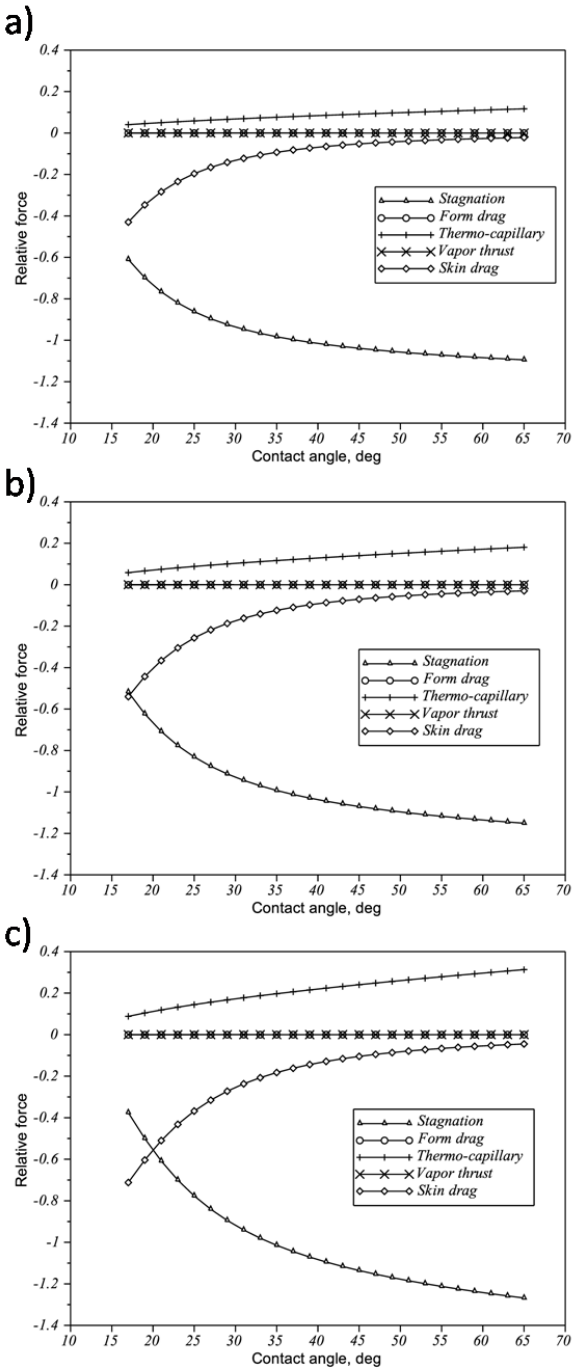

Figure 7: Relative force acting on a dry patch as a function of the contact angle for annular two-phase flow of steam-water mixture; assumed pressure gradient 1700 Pa/m, interfacial shear stress 8.8 Pa, wall heat flux= 1 MW/m^2 at: p = 2 MPa (a), p = 7 MPa (b), p = 12 MPa (c)

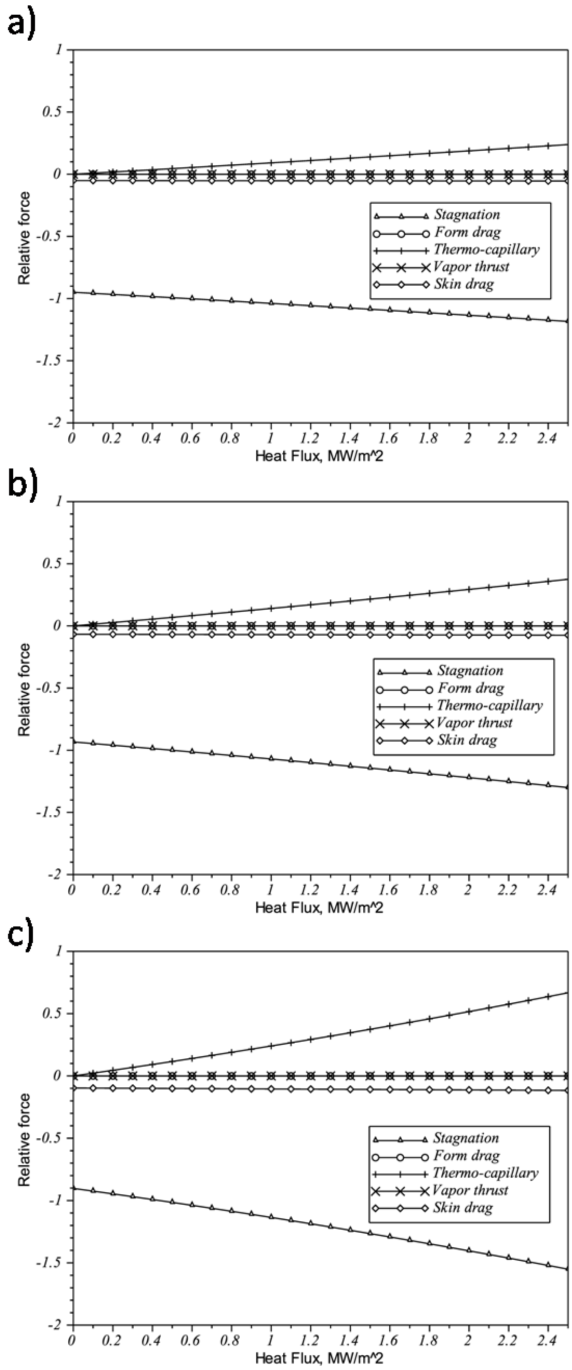

Figure 8: Relative force acting on a dry patch as a function of heat flux for annular two-phase flow of steam-water mixture; assumed pressure gradient 1700 Pa/m, interfacial shear stress 8.8 Pa, contact angle 45°C at: p = 2 MPa (a), p = 7 MPa (b), p = 12 MPa (c)

thermo-capillary and vapor thrust forces, the analysis includes the effects of the pressure gradient and the interfacial shear stress. The importance of turbulence in the liquid film is investigated by comparing results obtained with various turbulence models to the analytical solution valid for laminar flow as well as to selected experimental data.

It is concluded that the present model gives results which are in good agreement with experiments and analytical expressions given by Ponter et al. [16] and El-Genk and Saber [9] in the case of an isothermal liquid film flowing down a vertical surface. For adiabatic annular two-phase flow, the data obtained by Hewitt and Lacey [11] were used as a reference. The model correctly predicts a decreasing minimum wetting rate of a dry patch with increasing flow rate of the gas phase. The measured wetting rate could be matched with using the contact angle that was equal to one half of the static contact angle reported in the experiments. A sensitivity study indicates that the contact angle is the most sensitive parameter, whereas increasing turbulence level in the liquid film causes increased discrepancy between predictions and measurements.

The analyses performed for steam-water mixtures at various pressures indicate that the dominant forces which govern dry patch stability are due to the stagnation pressure and the surface tension effects. In the absence of other forces, the minimum wetting rate is governed by the balance between these two forces. With increasing heat flux, the importance of the thermo-capillary force grows and neglecting it may lead to a significant error. The fourth important force is skin friction. Its magnitude can be comparable to the stagnation force for small contact angles. This effect increases with increasing pressure of the two-phase mixture.

Acknowledgments

The publication was created in the framework of a strategic project of the Polish National Centre for Research and Development (NCBR): "Technologies for the development of safe nuclear energy", Research Task No. 9 entitled "Development and implementation of safety analysis methods in nuclear reactors during disturbances in heat removal and severe accident conditions”.

References

[1] G. F. Hewitt, A. H. Govan, Phenomenological modeling of non-equilibrium flows with phase change, Int. J. Heat Mass Transfer 33 (2) (1990) 229–242.

[2] C. Adamsson, H. Anglart, Influence of axial power distribution on dryout: Film flow models and experiments, Nucl. Eng. Des. 240 (2010) 1495–1505.

[3] T. Ueda, Y. Isayama, Critical heat flux and exit film flow rate in a flow boiling system, Int. J. Heat Mass Transfer 24 (7) (1981) 1267–1276.

[4] T. Fukano, S. Mori, T. Nakagawa, Fluctuation characteristics of heating surface temperature near an obstacle in transient boiling two-phase flow in a vertical annular channel, Nucl. Eng. Des. 219 (2003) 47–60.

[5] T. Hobler, Minimum surface wetting, Chemia Stosowana 2B (1964) 145–159.

[6] S. G. Bankoff, Minimum thickness of a draining liquid film, Int. J. Heat Mass Transfer 14 (1971) 2143–2146.

[7] J. Mikielewicz, J. R. Moszynski, Minimum thickness of a liquid film flowing down a solid surface, Int. J. Heat Mass Transfer 19 (1976) 771–776.

[8] A. Doniec, Laminar flow of a liquid rivulet down a vertical solid surface, Can. J. Chem. Eng. 69 (1991) 198–202.

[9] M. S. El-Genk, H. H. Saber, Minimum thickness of a flowing down liquid film on a vertical surface, Int. J. Heat Mass Transfer 44 (2001) 2809–2825.

[10] J. Mikielewicz, D. Mikielewicz, S. Gumkowski, A model of liquid film breakdown formed due to the impingement of a two-phase jet on a horizontal surface, Int. J. Heat Mass Transfer 53 (2010) 5456–5464.

[11] G. F. Hewitt, P. M. C. Lacey, The breakdown of the liquid film in annular two-phase flow, Int. J. Heat Mass Transfer 8 (1965) 781–791.

[12] D. E. Hartely, W. Murgatroyd, Criteria for the break-up of thin liquid layers flowing isothermally over solid surface, Int. J. Heat Mass Transfer 7 (1964) 1003–1015.

[13] N. Zuber, F. W. Staub, Stability of dry patches forming in liquid films flowing over heated surfaces, Int. J. Heat Mass Transfer 9 (1966) 897–905.

[14] G. D. McPherson, Axial stability of the dry patch formed in dryout of a two-phase annular flow, Int. J. Heat Mass Transfer 13 (1970) 1133–1152.

[15] F. Blanghetti, E. U. Shlunder, Local heat transfer coefficients on condensation in vertical tubes, in: Proc. 6th Int. Heat Transfer Conference, Vol. 2, 1978, pp. 437–442.

[16] B. Ponter, G. A. Davies, W. Beaton, T. K. Ross, The measurement of contact angles under conditions of heat transfer when a liquid film breaks on a vertical surface, Int. J. Heat Mass Transfer 10 (1967) 1633–1636.

[17] B. Ponter, G. A. Davies, T. K. Ross, P. G. Thornley, The influence of mass transfer on liquid film breakdown, Int. J. Heat Mass Transfer 10 (1967) 349–359.